Exploring Fairness for FAS-assisted Communication Systems: from NOMA to OMA

Junteng Yao, Liaoshi Zhou, Tuo Wu, Ming Jin, Cunhua Pan,
Maged Elkashlan, and Kai-Kit Wong, *Fellow*, *IEEE*

***Abstract*—This paper addresses the fairness issue within fluid antenna system (FAS)-assisted non-orthogonal multiple access (NOMA) and orthogonal multiple access (OMA) systems, focusing on scenarios where the base station (BS) transmits superposed signals to two users, each equipped with a single fluid antenna. We define fairness through the minimization of the maximum outage probability for two users, under total resource constraints for both FAS-assisted NOMA and OMA systems. Specifically, in the FAS-assisted NOMA systems, we differentiate between special and general cases, deriving a closed-form solution for the former and applying a bisection search method to find the optimal solution for the latter. For the general case, we also derive a locally optimal closed-form solution aiming at achieving fairness. In the realm of FAS-assisted OMA systems, to deal with non-convex optimization problem with the coupling of variables in the objective function, we employ an approximation strategy to facilitate a successive convex approximation (SCA)-based algorithm, achieving locally optimal solutions for both cases. Empirical analysis validates that our proposed solutions outperform conventional NOMA and OMA benchmarks in terms of fairness.**

***Index Terms*—Fairness, fluid antenna system, non-orthogonal multiple access, orthogonal multiple access.**

I. Introduction

A. Background

THE advent of sixth-generation (6G) wireless networks has significantly heightened the demand for massive connectivity across a broad spectrum of Internet of Things (IoT) applications, including industrial automation, environmental monitoring, and autonomous driving, evidencing a gradual increase [1], [2]. The limitations of single-antenna systems have led to the widespread adoption of the Multiple-Input Multiple-Output (MIMO) technique in IoT systems to enhance performance [3], [4], [5]. MIMO technology augments communication efficacy by generating spatial bandwidth, independent of frequency and time resources. Nonetheless, this approach is typically associated with increased energy consumption and hardware costs, attributed to the utilization of multiple antennas and radio frequency (RF) chains. In response to these challenges, the innovative concept of the fluid antenna system (FAS) has been introduced. This system, capable of dynamically selecting antenna positions across N locations (or ports), has been proposed as an effective means to achieve substantial space diversity while minimizing power consumption [6], [7].

J. Yao, L. Zhou, and M. Jin are with the Faculty of Electrical Engineering and Computer Science, Ningbo University, Ningbo 315211, China (e-mail: yaojunteng@nbu.edu.cn, zls1045866546@163.com, and jinming@nbu.edu.cn).

T. Wu and M. Elkashlan are with the School of Electronic Engineering and Computer Science at Queen Mary University of London, London E1 4NS, U.K. (e-mail: tuo.wu@qmul.ac.uk).

C. Pan is with the National Mobile Communications Research Laboratory, Southeast University, Nanjing 210096, China. (e-mail: cpan@seu.edu.cn).

K.-K. Wong is with the Department of Electronic and Electrical Engineering, University College London, WC1E 6BT London, U.K., and also with the Yonsei Frontier Laboratory and the School of Integrated Technology, Yonsei University, Seoul 03722, South Korea (e-mail: kat-kit.wong@ucl.ac.uk).

B. Related Work

Unlike MIMO systems, which typically utilize multiple fixed-position antennas, the FAS incorporates only a single RF chain, thereby reducing energy consumption. The fluid antenna (FA) comprises liquid metals, encompassing both movable and non-movable flexible antennas [8], [9]. Leveraging the flexibility of liquid metals, FAS can selectively navigate across a designated area with multiple ports. This adaptability and the ability to configure the wireless communication channel have recently garnered significant research interest [10], [11], [12], [13], [14], [15], [16], [17], [18], [19]. Wong *et al.* [10] explored the outage probability in point-to-point FAS deployments, where the receiver is equipped with a single FA, demonstrating superior performance of FAS over traditional multiple-antenna maximum ratio combining (MRC) systems with a large number of ports. Building on this, Lai *et al.* [11] examined the outage performance of FAS by initially selecting the optimal ports, followed by signal combination using the MRC technique. Recognizing the importance of channel estimation for FAS, Xu *et al.* [12] introduced a new channel estimation scheme for millimeter-wave (mmWave) systems, utilizing the port selection feature of FA. Addressing optimal port selection, Chai *et al.* [13] developed a machine learning-based method that achieves exceptional performance with a minimal set of observed ports. Integrating FA into MIMO systems significantly enhances communication performance; Ye *et al.* [14] optimized both the port position and transmit beamforming at the base station (BS) to maximize transmission rates. Considering physical layer security (PLS) within FAS, Tang *et al.* [15] focused on maximizing the secrecy rate for legitimate users by optimizing the power allocation between legitimate signals and artificial noise (AN).

The aforementioned studies primarily focused on communication between the BS and one registered user or one legitimate user. However, addressing communication in scenarios involving multiple users is crucial. To evaluate the performance of the FAS within the multi-user scenario, Wong *et al.* [16] introduced the concept of fluid antenna multiple

access (FAMA), characterizing the multiple access capability of FAS. In this study, the authors employed the signal-to-interference ratio (SINR) to derive the closed-form outage probability for users. Given the impracticality of each user selecting its optimal port during each symbol duration in FAMA, Wong *et al.* [17] subsequently developed the concept of slow FAMA (s-FAMA), allowing users to select their best port within the channel fading block. To facilitate port selection in s-FAMA, Waqar *et al.* [18] introduced a deep learning-based port selection method, significantly reducing complexity. Additionally, user scheduling has been identified as a method to enhance FAMA's performance; hence, Wong *et al.* [19] proposed opportunistic FAMA, enabling the selection of favorable users. Although effective user scheduling can mitigate the outage probability in FAS multiple access, interference among the plethora of wireless mobile devices remains a significant challenge.

To manage interference amidst the extensive connectivity in FAS, orthogonal multiple access (OMA) emerges as a viable solution for serving multiple users. In OMA systems, users are allocated orthogonal resource blocks, such as time, frequency, and code, eliminating inter-user interference. However, the orthogonal nature of OMA inherently limits the number of accessible users. Additionally, channel fading often disrupts this orthogonality [20], [21]. Addressing these limitations, non-orthogonal multiple access (NOMA) has been identified as an efficient strategy for supporting a large number of users within the same resource block [20], [21], [22]. NOMA operates by transmitting superposed signals, with receivers decoding their intended signals through the successive interference cancellation (SIC) technique, thereby effectively managing interference [23], [24].

Research on NOMA systems categorizes channel state information (CSI) at the transmitter into three types: perfect CSI [25], [26], [27], partial CSI [28], [29], [30], and statistical CSI [31], [32], [33]. Specifically, Li in *et al.* [25] worked on maximizing the downlink NOMA system's achievable rate for users distant from the BS by optimizing BS transmit beamforming under perfect CSI assumptions.. Besides, [26] tackled the weighted sum throughput maximization in multicarrier NOMA systems, allocating each subcarrier to a maximum of two users in both downlink and uplink. For partial CSI, Hou *et al.* in [28] introduced a clustering strategy enhancing the NOMA system coverage with only partial CSI required. Additionally, the authors of [29] explored user scheduling in NOMA systems with limited feedback, while Yapici *et al.* assessed the outage performance in NOMA systems utilizing mmWave communications with one-bit quantized feedback in [30]. Regarding statistical CSI, Ding *et al.* calculated NOMA systems' outage probability and achievable rate using a 2D homogeneous Poisson point process (PPP) for BS and user modeling in [31]. Building upon this, Wang *et al.* aimed at maximizing sum throughput in NOMA systems under Nakagami-m fading channels through strategic power allocation [32]. Lastly, Li *et al.* evaluated the outage performance in multi-carrier downlink NOMA systems based on statistical CSI, defining outage as the condition when a user's sum rate across subcarriers falls below a specific target rate in [33].

The above mentioned works demonstrated the superiority of OMA systems and NOMA systems. Therefore, it is envisioned that enabling the OMA and NOMA technique in FAS can further improve the quality of services (QoS) [34], [35], [36], [37]. Hence, Skouroumounis *et al.* in [34] studied the tradeoff between channel estimation and outage probability in the FAS-assisted time-division multiple access (TDMA) systems by using the stochastic geometry method. The authors of [35] analyzed the outage performance of the FAS-assisted cooperative NOMA systems, where the central user (CU) serves as a relay for forwarding the signals to the cell-edge users (EUs), while Zheng *et al.* investigated the outage performance of the FAS-assisted NOMA systems with short-packet communications in [36]. The authors of [37] maximized the sum rate in the FAS-assisted NOMA systems by jointly designing port selection and power allocation subject to per-user QoS.

C. Motivations and Contributions

The aforementioned studies underscored the significant benefits of the FAS on both OMA and NOMA systems. However, these investigations commonly assumed the availability of perfect instantaneous CSI at the transmitter, an assumption that is impractical due to the challenges in acquiring accurate CSI caused by non-ideal feedback channels and delays. Moreover, while the assumption of partial CSI availability presents a more realistic scenario, it significantly complicates the power allocation process in NOMA systems due to the uncertainty in the ordering of channel gains. Consequently, we adopt a more realistic scenario, namely, statistical CSI. In this context, the outage performance of OMA and NOMA systems emerges as an appropriate metric for analysis and optimization.

In FAS-assisted communication systems, ensuring fairness is crucial for effectively guaranteeing users' quality of service (QoS) and reducing the outage performance of both FAS-assisted communication systems [34], [35], [36]. The challenge of resource allocation becomes particularly acute under the constraints of limited resources. In NOMA systems, where superposition signals are concurrently transmitted to different users within the same source blocks, inter-user interference is inevitable. A limited total power budget necessitates that enhancing one user's signal strength comes at the expense of others, leading to higher outage probabilities for users with weakened signal power [40], [38], [39]. Thus, investigating fairness within FAS-assisted NOMA systems is essential.

Similarly, in FAS-assisted OMA systems, where signals for individual users are transmitted independently across orthogonal source blocks, the principle of fairness remains critical. Despite the challenges posed by total resource constraints, maintaining fairness among users is imperative, as it significantly impacts the equitable optimization of system performance [40].

Hence, this paper is dedicated to exploring the fairness within the FAS-assisted NOMA and OMA communication systems. The main contributions of this study are outlined below:

- This paper investigates a FAS-assisted NOMA and OMA system, where the BS is equipped with a single conventional antenna, and the CU and the EU are both

equipped with a single fluid antenna. Assuming that the BS only knows the statistical CSI of two users, we aim to minimize the maximum outage probability of two users in two different systems by designing the corresponding resource allocation.

- In FAS-assisted NOMA systems, we examine both a special and a general case. In the special case, we presume identical parameters, such as the number of ports and correlation factors, across two users. Here, we theoretically demonstrate the existence of a unique optimal closed-form solution. Conversely, in the general case, deriving a closed-form solution proves challenging due to the involvement of the integral of the first-order Marcum Q function in the expression of users' outage probabilities. To overcome this, we employ a bisection search algorithm, leveraging the monotonic relationship of the outage probabilities with the power allocation coefficient, to find the optimal solution. Additionally, to minimize computational complexity, we introduce an approximate expression for the objective function and derive a locally optimal solution in closed form for the general case.
- In FAS-assisted OMA systems, we specifically focus on TDMA systems. The considered problem is non-convex due to the coupling of the time allocation and power allocation coefficients within the objective function, rendering the method proposed for NOMA systems ineffective. Furthermore, the formulation of this objective function presents considerable computational difficulties. To tackle this challenge, we approximate the objective function and introduce a Successive Convex Approximation (SCA) algorithm to derive a locally optimal solution for both special and general cases.
- The numerical results demonstrate that our proposed schemes surpass the benchmark schemes in both conventional NOMA and OMA systems in terms of outage performance.

The rest of this paper is organized as follows. Section II introduces the system model for the FAS-assisted downlink NOMA system. In Section III, the special case and the general case in the NOMA systems are considered, and the closed-form solution and the optimal solution based the bisection search algorithm are proposed. In Section IV, we described the system model for the FAS-assisted OMA systems, and proposed the SCA-based algorithm to obtain the sub-optimal solution for two cases. Simulation results and discussion are provided in Section V. Finally, conclusions are drawn in Section VI.

II. System Model

Consider a FAS-assisted NOMA system, which consists of a BS equipped with a single traditional antenna, a CU near the BS, and an EU far from the BS. Both CU and EU are equipped with a single fluid antenna to receive signals from the BS. Both the CU and the EU have the capability to dynamically switch their fluid antennas to the most favorable port among a total of K and M ports, respectively. These ports are evenly distributed across linear spaces of sizes $W_c\lambda$ for the CU and $W_e\lambda$ for the EU, where λ represents the wavelength. This arrangement facilitates optimal antenna positioning for both users, enhancing signal reception by leveraging the spatial diversity provided by the multiple ports. Moreover, it is assumed that the time delays resulting from port switching are insignificantly small [6], [16].

A. Channel Model

In the FAS-assisted NOMA system under consideration, the communication channels from the BS to the k-th port of the CU and the m-th port of the EU are represented by h_k and g_m, respectively, where $k = 1, \ldots, K$ and $m = 1, \ldots, M$, $K \geq 2$ and $M \geq 2$. The specific mathematical expressions for these channels are expressed as [10], [17]

$$h_k = \mu_h h_0 + (1-\mu_h) z_k, \tag{1}$$

$$g_m = \mu_g g_0 + (1-\mu_g) \nu_m. \tag{2}$$

Here, the channel parameters for the virtual reference ports, h_0 for the CU and g_0 for the EU, are characterized by complex Gaussian distributions $\mathcal{CN}(0, \sigma_h^2)$ and $\mathcal{CN}(0, \sigma_g^2)$, respectively. Both have zero means and variances of σ_h^2 and σ_g^2. Furthermore, the terms z_k and ν_j, representing independently and identically distributed (i.i.d.) random variables for the CU and EU respectively, also follow complex Gaussian distributions with $\mathcal{CN}(0, \sigma_h^2)$ and $\mathcal{CN}(0, \sigma_g^2)$. Additionally, μ_h and μ_g represent the correlation factors, which are respectively given by [10], [17]

$$\mu_h = \sqrt{2}\sqrt{{}_1F_2\left(\frac{1}{2}; 1; \frac{3}{2}; -\pi^2 W_c^2\right) - \frac{J_1(2\pi W_c)}{2\pi W_c}}, \tag{3}$$

$$\mu_g = \sqrt{2}\sqrt{{}_1F_2\left(\frac{1}{2}; 1; \frac{3}{2}; -\pi^2 W_e^2\right) - \frac{J_1(2\pi W_e)}{2\pi W_e}}, \tag{4}$$

where ${}_aF_b$ denotes the generalized hypergeometric function and $J_1(\cdot)$ represents the first-order Bessel function of the first kind.

Given $|h_0|$, the probability density function (PDF) of h_k can be expressed as

$$f_{|h_k|\left||h_0|\right.}(r_n|r_0) = \frac{2r_k}{\sigma_h^2(1-\mu_h^2)} e^{-\frac{r_n^2+\mu_h^2 r_0^2}{\sigma_h^2(1-\mu_h^2)}} I_0\left(\frac{2\mu_h r_k r_0}{\sigma_h^2(1-\mu_h^2)}\right), \tag{5}$$

where $I_0(u)$ denotes the modified Bessel function of the first kind and order zero. The series representation of this function is given by [41]

$$I_0(z) = \sum_{a=0}^{\infty} \frac{z^{2a}}{2^{2a} a! \Gamma(a+1)}, \tag{6}$$

noting that $\Gamma(a+1) = a!$.

Similarly, with $|g_0|$ given, the PDF of g_m can be expressed as

$$f_{|g_m|\left||g_0|\right.}(r_m|r_0) = \frac{2r_m}{\sigma_g^2(1-\mu_g^2)} e^{-\frac{r_m^2+\mu_g^2 r_0^2}{\sigma_g^2(1-\mu_g^2)}} I_0\left(\frac{2\mu_g r_m r_0}{\sigma_g^2(1-\mu_g^2)}\right). \tag{7}$$

B. Signal Model

Building upon the NOMA protocol, the signal transmitted from the BS can be formulated as

$$x = \sqrt{P\alpha}x_c + \sqrt{P(1-\alpha)}x_e, \tag{8}$$

where P denotes the transmit power at the BS, and α represents the power allocation coefficient for the CU. The terms x_c and x_e correspond to the independent, information-bearing signals intended for the CU and EU, respectively. It is assumed that both signals are normalized, satisfying $\mathbf{E}[|x_c|] = \mathbf{E}[|x_e|] = 1$.

In this context, let us denote the signals received at the CU and EU as y_k and y_m, respectively. These received signals are defined by the following equations:

$$y_k = h_k x + n_k, \tag{9}$$

$$y_m = g_m x + n_m, \tag{10}$$

where h_k and g_m denote the quasi-static fading channel parameters from the BS to the k-th port of the CU and the m-th port of the EU, respectively. Furthermore, $n_k \sim \mathcal{CN}(0, \sigma^2)$ and $n_m \sim \mathcal{CN}(0, \sigma^2)$ represent the independent additive Gaussian noises at the CU and EU, respectively.

Upon receiving the signal y_k, the CU employs the successive interference cancellation (SIC) scheme to first decode x_e by regarding x_c as interference. The corresponding signal-to-noise-plus-interference ratio (SINR) for this process is expressed as

$$\gamma_{c,e} = \frac{P(1-\alpha)|h_c|^2}{P\alpha|h_c|^2 + \sigma^2}. \tag{11}$$

Given that x_e is successfully decoded by the CU, the CU then proceeds to decode x_c. The signal-to-noise ratio (SNR) for decoding x_c is given by

$$\gamma_c = \frac{P\alpha|h_c|^2}{\sigma^2}. \tag{12}$$

Additionally, it is assumed that the CU can swiftly switch its fluid antenna to the most advantageous port, thereby achieving the maximum value of $|h_k|$. This maximum value can be mathematically expressed as

$$|h_{\max}| = \max\{|h_1|, |h_2|, \cdots, |h_K|\}. \tag{13}$$

Building upon this, the outage probability at the CU is given by

$$\begin{aligned}\mathbf{P}_{\mathrm{c}}^{\mathrm{out}} =& 1 - \mathbf{P}(|h_{\max}|^2 > \max\{\phi_1, \phi_2\}) \\ =& \int_0^\infty e^{-t} \cdot \left[1 - Q_1\left(\sqrt{\frac{2\mu_h^2}{1-\mu_h^2}}\sqrt{t}, \right.\right. \\ & \left.\left. \sqrt{\frac{2}{1-\mu_h^2}}\sqrt{\frac{\max\{\phi_1, \phi_2\}}{\sigma_h^2}}\right)\right]^K dt,\end{aligned} \tag{14}$$

where

$$\phi_1 = \frac{\gamma_{th,2}\sigma^2}{P(1-\alpha-\gamma_{th,2}\alpha)}, \tag{15}$$

$$\phi_2 = \frac{\gamma_{th,1}\sigma^2}{P\alpha}, \tag{16}$$

$\gamma_{th,1} = 2^{R_1} - 1$ and $\gamma_{th,2} = 2^{R_2} - 1$, R_1 and R_2 are the targeted rate of x_c and x_e, respectively.

From (15), we know that $\phi_1 > 0$ when $\alpha < \frac{1}{1+\gamma_{th,2}}$, and $\mathbf{P}_c^{\text{out}} = 1$ when $\phi_1 \leq 0$. Combining (15) with (16), we know that $\phi_1 > \phi_2$ when $\frac{1}{1+\gamma_{th,2}+\gamma_{th,2}/\gamma_{th,1}} < \alpha < \frac{1}{1+\gamma_{th,2}}$, $\phi_1 \leq \phi_2$ when $0 < \alpha \leq \frac{1}{1+\gamma_{th,2}+\gamma_{th,2}/\gamma_{th,1}}$.

For the EU, after receiving the signal y_m, it decodes x_e by treating x_c as interference, the corresponding SINR is given by

$$\gamma_e^m = \frac{P(1-\alpha)|g_m|^2}{P\alpha|g_m|^2 + \sigma^2}. \tag{17}$$

Additionally, it is assumed that the EU can swiftly switch its fluid antenna to the optimal port. Consequently, the maximum value of $|g_m|$ can be expressed as

$$|g_{\max}| = \max\{|g_1|, |g_2|, \cdots, |g_M|\}. \tag{18}$$

The outage probability at EU can be expressed as follows:

$$\begin{aligned}\mathbf{P}_e^{\text{out}} =& 1 - \mathbf{P}(|g_{\max}|^2 > \phi_1) \\ =& \int_0^\infty e^{-t}\left[1 - Q_1\left(\sqrt{\frac{2\mu_g^2}{1-\mu_g^2}}\sqrt{t}, \right.\right. \\ & \left.\left. \sqrt{\frac{2}{1-\mu_g^2}}\sqrt{\frac{\phi_1}{\sigma_g^2}}\right)\right]^M dt,\end{aligned} \tag{19}$$

C. Problem Formulation

To enhance the spectrum efficiency of the NOMA system, addressing the fairness issue is crucial when optimizing the overall communication performance of the considered systems. Based on the fairness criterion, we consider the min-max outage probability fairness problem in this paper. The considered problem can be formulated as

$$\begin{aligned}&\min_{\alpha} \ \max\{\mathbf{P}_c^{\text{out}}, \mathbf{P}_e^{\text{out}}\} \\ &\text{s.t. } 0 < \alpha < \frac{1}{1+\gamma_{th,2}}.\end{aligned} \tag{20}$$

According to (15) and (16), Problem (20) can be decomposed into the following two sub-problems.

$$\begin{aligned}\text{(P1)} \quad &\min_{\alpha} \ \max\{\mathbf{P}_c^{\text{out}}(\phi_2), \mathbf{P}_e^{\text{out}}\} \\ &\text{s.t. } 0 < \alpha \leq \frac{1}{1+\gamma_{th,2}+\gamma_{th,2}/\gamma_{th,1}},\end{aligned} \tag{21}$$

and

$$\begin{aligned}\text{(P2)} \quad &\min_{\alpha} \ \max\{\mathbf{P}_c^{\text{out}}(\phi_1), \mathbf{P}_e^{\text{out}}\} \\ &\text{s.t. } \frac{1}{1+\gamma_{th,2}+\gamma_{th,2}/\gamma_{th,1}} < \alpha < \frac{1}{1+\gamma_{th,2}},\end{aligned} \tag{22}$$

where

$$\mathbf{P}_c^{\text{out}}(\phi_1) = \int_0^\infty e^{-t}\left[1 - Q_1\left(\sqrt{\frac{2\mu_h^2}{1-\mu_h^2}}\sqrt{t}, \sqrt{\frac{2}{1-\mu_h^2}}\sqrt{\frac{\phi_1}{\sigma_h^2}}\right)\right]^K dt, \quad (23)$$

$$\mathbf{P}_c^{\text{out}}(\phi_2) = \int_0^\infty e^{-t}\left[1 - Q_1\left(\sqrt{\frac{2\mu_h^2}{1-\mu_h^2}}\sqrt{t}, \sqrt{\frac{2}{1-\mu_h^2}}\sqrt{\frac{\phi_2}{\sigma_h^2}}\right)\right]^M dt. \quad (24)$$

III. Min-Max Fairness for NOMA Systems

In this section, we aim to solve Problem (20) in two different cases according to the situation of the FAS within the CU and that within the EU. In this context, we can deduce several insights for the considered FAS-assisted NOMA systems.

A. Special Case

In this subsection, we examine a particular scenario where $K = M = N$ and $\mu_h = \mu_g = \mu$. Under this condition, we first investigate the monotonicity of $\mathbf{P}_c^{\text{out}}(\phi_1)$, $\mathbf{P}_c^{\text{out}}(\phi_2)$, and $\mathbf{P}_e^{\text{out}}$ with respect to α, as detailed in the subsequent lemma.

Lemma 1: $\mathbf{P}_c^{\text{out}}(\phi_2)$ decreases with α, whereas $\mathbf{P}_c^{\text{out}}(\phi_1)$ and $\mathbf{P}_e^{\text{out}}$ increase with α.

Proof: Refer to Appendix A. ■

Leveraging the monotonicity established in *Lemma 1*, the following lemma addresses Problem (20).

Lemma 2: The optimal solution for Problem (20) is $\frac{1}{1+\gamma_{th,2}+\frac{\gamma_{th,2}\sigma_h^2}{\gamma_{th,1}\sigma_g^2}}$.

Proof: Refer to Appendix B. ■

Remark 1: The optimal solution identified in (74) for this specific case aligns with that of traditional NOMA using a conventional single antenna. Thus, when the number of ports for the CU and EU are equal, the optimization algorithm from traditional NOMA approaches can be adapted.

B. General Case

In this subsection, the analysis extends to a general scenario where $N_e \neq N_c$ or $\mu_h \neq \mu_g$, aiming to resolve Problem (20).

Drawing from *Lemma 1* with the special case, the monotonic behaviors of $\mathbf{P}_c^{\text{out}}(\phi_2)$, $\mathbf{P}_c^{\text{out}}(\phi_1)$, and $\mathbf{P}_e^{\text{out}}$ in relation to α are consistent in the general case. Consequently, given that the solution to Problem (20) coincides with that of Problem (21), we deduce that these problems are effectively synonymous.

However, given the differences $N_e \neq N_c$ and $\mu_h \neq \mu_g$, we cannot assert that $\mathbf{P}_c^{\text{out}}(\phi_2) = \mathbf{P}_c^{\text{out}}(\phi_1) < \mathbf{P}_e^{\text{out}}$ under the condition $\alpha = \frac{1}{1+\gamma th,2+\gamma th,2/\gamma th,1}$, as proposed in the special case. Notably, when $\alpha = 0$, $\mathbf{P}_e^{\text{out}} < \mathbf{P}_c^{\text{out}}(\phi_2) = 1$, leading to the identification of optimal solutions for Problem (21) in the following two conditions:

Condition 1: The optimal α is $\frac{1}{1+\gamma_{th,2}+\gamma_{th,2}/\gamma_{th,1}}$ if $\mathbf{P}_c^{\text{out}}(\phi_2) \geq \mathbf{P}_e^{\text{out}}$ at this α value;

Condition 2: The optimal α lies within $\left(0, \frac{1}{1+\gamma_{th,2}+\gamma_{th,2}/\gamma_{th,1}}\right)$ if $\mathbf{P}_c^{\text{out}}(\phi_2) < \mathbf{P}_e^{\text{out}}$ at the specified α.

For *Condition 2*, a unique value of α exists that equates $\mathbf{P}_c^{\text{out}}(\phi_2)$ with $\mathbf{P}_e^{\text{out}}$. To determine the optimal α under *Condition 2*, the bisection search method is employed within the interval $\left(0, \frac{1}{1+\gamma_{th,2}+\gamma_{th,2}/\gamma_{th,1}}\right)$.

Complexity Analysis: The complexity of solving Problem (21) is

$$\mathcal{O}\left(\log \frac{1}{(1+\gamma_{th,2}+\gamma_{th,2}/\gamma_{th,1})\delta}\right), \quad (25)$$

where δ is the accuracy of the bisection search.

The complexity analysis above reveals that the computational complexity of utilizing the bisection search method is considerable. To further reduce computational complexity, we introduce a method based on a closed-form solution to address Problem (21). Specifically, for $\mathbf{P}_c^{\text{out}}(\phi_2)$, given that $0 \leq Q_1\left(\sqrt{\frac{2\mu_h^2}{1-\mu_h^2}}\sqrt{t}, \sqrt{\frac{2}{1-\mu_h^2}}\sqrt{\frac{\phi_2}{\sigma_h^2}}\right) \leq 1$, the following approximation can be derived:

$$\left[1 - Q_1\left(\sqrt{\frac{2\mu_h^2}{1-\mu_h^2}}\sqrt{t}, \sqrt{\frac{2}{1-\mu_h^2}}\sqrt{\frac{\phi_2}{\sigma_h^2}}\right)\right]^{N_c} \approx 1 - N_c Q_1\left(\sqrt{\frac{2\mu_h^2}{1-\mu_h^2}}\sqrt{t}, \sqrt{\frac{2}{1-\mu_h^2}}\sqrt{\frac{\phi_2}{\sigma_h^2}}\right). \quad (26)$$

Consequently, by using

$$\int_0^c e^{-t}Q_1(a\sqrt{t}, b)dt = e^{-\frac{b^2}{a^2+2}}Q_1\left(\sqrt{c(a^2+2)}, \frac{ab}{\sqrt{a^2+2}}\right) - e^{-c}Q_1(a\sqrt{c}, b), \quad (27)$$

$\mathbf{P}_c^{\text{out}}(\phi_2)$ can be approximated by

$$\tilde{\mathbf{P}}_c^{\text{out}}(\phi_2) = 1 - N_c e^{-\frac{\phi_2}{\sigma_h^2}}. \quad (28)$$

Similarly, $\mathbf{P}_e^{\text{out}}$ can be approximated as follows:

$$\tilde{\mathbf{P}}_e^{\text{out}} = 1 - N_e e^{-\frac{\phi_1}{\sigma_g^2}}. \quad (29)$$

Drawing parallels to *Lemma* 1, it becomes apparent that $\tilde{\mathbf{P}}_c^{\text{out}}(\phi_2)$ decreases with α, whereas $\tilde{\mathbf{P}}_e^{\text{out}}$ increases with α. Consequently, the optimal solution to Problem (21) is achieved when $\tilde{\mathbf{P}}_c^{\text{out}}(\phi_2) = \tilde{\mathbf{P}}_e^{\text{out}}$. This leads to the following theorem.

Theorem 1: For the solution to Problem (21),

- When $N_c = N_e$, the closed-form solution is

$$\tilde{\alpha} = \frac{1}{1+\gamma_{th,2}+\frac{\gamma_{th,2}\sigma_h^2}{\gamma_{th,1}\sigma_g^2}}. \quad (30)$$

- When $N_c \neq N_e$, and both $\alpha_1 \geq 0$ and $\alpha_2 \geq 0$ are real values, the closed-form solution is

$$\tilde{\alpha} = \min\left\{\min\left\{[\alpha_1]^+, \frac{1}{1+\gamma_{th,2}+\frac{\gamma_{th,2}}{\gamma_{th,1}}}\right\}, \min\left\{[\alpha_2]^+, \frac{1}{1+\gamma_{th,2}+\frac{\gamma_{th,2}}{\gamma_{th,1}}}\right\}\right\}, \quad (31)$$

where $[z]^+$ denotes $\max\{z, 0\}$, and α_1 and α_2 are determined by (81) and (82), respectively.

Proof: See Appendix C. ■

If α_1 or α_2 are not real values, they are set to $+\infty$. Similarly, if $\alpha_1 < 0$ or $\alpha_2 < 0$, they are also set to $+\infty$. The optimal solution is thereby determined by (31).

Remark 2: When $N_c = N_e$, the optimal solution given by (80) aligns with the solution in (74) for the special case.

IV. Min-Max Fairness for OMA Systems

In this section, we extend our investigation to conventional OMA systems, i.e., TDMA, to provide a comprehensive understanding of fairness issues within FAS-assisted communication systems. To be specific, we delve into the fairness optimization problem in OMA systems, which serves as a benchmark for comparing these systems against NOMA systems.

A. Problem Formulation

Based on the TDMA protocol, the SNR at the CU and the EU can be expressed as

$$\gamma_{c,\text{OMA}}^{k} = \frac{P\alpha|h_k|^2}{\sigma^2}, \tag{32}$$

$$\gamma_{e,\text{OMA}}^{m} = \frac{P(1-\alpha)|g_m|^2}{\sigma^2}. \tag{33}$$

Then, by denoting the normalized time allocation coefficient for the CU as β (where $0 < \beta < 1$), the achievable rates of CU and EU can be derived as

$$R_c = \beta \log_2\left(1 + \max\{\gamma_{c,\text{OMA}}^{k}\}\right), \tag{34}$$

$$R_e = (1-\beta)\log_2\left(1 + \max\{\gamma_{e,\text{OMA}}^{m}\}\right). \tag{35}$$

Accordingly, the outage probability at the CU and the EU can be written as

$$\mathbf{P}_{c,\text{OMA}}^{\text{out}} = \int_0^\infty e^{-t}\cdot\left[1 - Q_1\left(\sqrt{\frac{2\mu_h^2}{1-\mu_h^2}}\sqrt{t}, \sqrt{\frac{2}{1-\mu_h^2}}\sqrt{\frac{\psi_1}{\sigma_h^2}}\right)\right]^{N_c} dt, \tag{36}$$

$$\mathbf{P}_{e,\text{OMA}}^{\text{out}} = \int_0^\infty e^{-t}\cdot\left[1 - Q_1\left(\sqrt{\frac{2\mu_g^2}{1-\mu_g^2}}\sqrt{t}, \sqrt{\frac{2}{1-\mu_g^2}}\sqrt{\frac{\psi_2}{\sigma_g^2}}\right)\right]^{N_e} dt, \tag{37}$$

where $\psi_1 = \frac{\bar{\gamma}_{th,1}\sigma^2}{P\alpha}$, $\psi_2 = \frac{\bar{\gamma}_{th,2}\sigma^2}{P(1-\alpha)}$, $\bar{\gamma}_{th,1} = 2^{\frac{R_1}{\beta}} - 1$ and $\bar{\gamma}_{th,2} = 2^{\frac{R_2}{1-\beta}} - 1$. Therefore, the min-max fairness optimization problem in OMA systems can be formulated as

$$\min_{0<\alpha<1, 0<\beta<1} \max\{\mathbf{P}_{c,\text{OMA}}^{\text{out}}, \mathbf{P}_{e,\text{OMA}}^{\text{out}}\}. \tag{38}$$

B. SCA-Based Algorithm

Due to the coupling of optimization variables in the objective function, Problem (38) is non-convex. The interdependence of α and β in $\mathbf{P}_{c,\text{OMA}}^{\text{out}}$ and $\mathbf{P}_{e,\text{OMA}}^{\text{out}}$ renders the closed-form solution for special case and the bisection search for general case inapplicable to OMA systems. To solve Problem (38), we introduce a successive convex approximation (SCA)-based algorithm to derive a locally optimal solution for both cases.

We begin by deriving the approximations for $\mathbf{P}_c^{\text{out}}$ and $\mathbf{P}_e^{\text{out}}$. Following (7), the approximation for $f_{|g_m||g_0|}(r_m|r_0)$ is given by

$$\hat{f}_{|g_m||g_0|}(r_m|r_0) = \frac{2r_m}{\sigma_g^2(1-\mu_g^2)} e^{-\frac{r_m^2+\mu_g^2 r_0^2}{\sigma_g^2(1-\mu_g^2)}}, \tag{39}$$

when $I_0(z) \approx 1$.

Considering $|g_0|$, it is evident that $|g_1|, \ldots, |g_M|$ are mutually independent. This independence allows us to deduce the approximate joint PDF of $|g_1|, \ldots, |g_M|$ given $|g_0|$ as

$$\hat{f}_{|g_1|,\ldots,|g_{N_e}|||g_0|}(r_1, \ldots, r_M \mid r_0) = \prod_{k=1}^{M} \frac{2r_k}{\sigma_g^2(1-\mu_g^2)} e^{-\frac{r_k^2+\mu_g^2 r_0^2}{\sigma_g^2(1-\mu_g^2)}}. \tag{40}$$

Consequently, the approximate joint PDF of $|g_0|, \ldots, |g_M|$ can be expressed as

$$\hat{f}_{|g_0|,\ldots,|g_M|}(r_0, \ldots, r_M) = \frac{2r_0}{\sigma_g^2} e^{-\frac{r_0^2}{\sigma_g^2}} \prod_{m=1}^{M} \frac{2r_m}{\sigma_g^2(1-\mu_g^2)} e^{-\frac{r_m^2+\mu_g^2 r_0^2}{\sigma_g^2(1-\mu_g^2)}}. \tag{41}$$

Building upon (41), the approximations of $\mathbf{P}_{c,\text{OMA}}^{\text{out}}$ and $\mathbf{P}_{e,\text{OMA}}^{\text{out}}$ are given by

$$\hat{\mathbf{P}}_{c,\text{OMA}}^{\text{out}} \approx \eta_h \left[1 - e^{-\frac{\psi_1}{\sigma_h^2(1-\mu_h^2)}}\right]^{N_c}, \tag{42}$$

$$\hat{\mathbf{P}}_{e,\text{OMA}}^{\text{out}} \approx \eta_g \left[1 - e^{-\frac{\psi_2}{\sigma_g^2(1-\mu_g^2)}}\right]^{N_e}, \tag{43}$$

where $\eta_h = \frac{1-\mu_h^2}{1+(N_c-1)\mu_h^2}$, and $\eta_g = \frac{1-\mu_g^2}{1+(N_e-1)\mu_g^2}$.

By introducing a slack variable τ and leveraging the approximations in (44) and (43), Problem (38) can be rewritten as

$$\min_{\alpha, 0<\rho} \quad \tau \tag{44a}$$

$$\text{s.t.} \quad \hat{\mathbf{P}}_{c,\text{OMA}}^{\text{out}} \le \tau, \tag{44b}$$

$$\hat{\mathbf{P}}_{e,\text{OMA}}^{\text{out}} \le \tau. \tag{44c}$$

$$0 < \alpha < 1, \tag{44d}$$

$$0 < \beta < 1. \tag{44e}$$

However, Problem (44) is still a non-convex problem due to the non-convex constraints (44b) and (44c). To address this issue, we further introduce two slack variables,i.e., a and b. Consequently, constraints (44b) and (44c) can be reformulated as

$$1 - a \le \left(\frac{\tau}{\eta_h}\right)^{\frac{1}{N_c}} \text{ and } 1 - b \le \left(\frac{\tau}{\eta_g}\right)^{\frac{1}{N_e}}, \tag{45}$$

$$a \le e^{-\frac{\psi_1}{\sigma_h^2(1-\mu_h^2)}} \text{ and } b \le e^{-\frac{\psi_2}{\sigma_g^2(1-\mu_g^2)}}. \tag{46}$$

For constraints (45), we have the following lemma.

Lemma 3: The constraints in (45) are convex.

Proof: By taking the first-order partial derivative and the second-order partial derivative of $\left(\frac{\tau}{\eta_g}\right)^{\frac{1}{N_e}}$ with respect to τ, we have

$$\frac{\partial\left(\frac{\tau}{\eta_g}\right)^{\frac{1}{N_e}}}{\partial\tau}=\frac{1}{\eta_g N_e}\left(\frac{\tau}{\eta_g}\right)^{\frac{1-N_e}{N_e}}, \tag{47}$$

$$\frac{\partial^2\left(\frac{\tau}{\eta_g}\right)^{\frac{1}{N_e}}}{\partial\tau^2}=\frac{1-N_e}{\eta_g^2 N_e^2}\left(\frac{\tau}{\eta_g}\right)^{\frac{1-2N_e}{N_e}}. \tag{48}$$

Because $N_e > 1$, $\frac{\partial^2\left(\frac{\tau}{\eta_g}\right)^{\frac{1}{N_e}}}{\partial\tau^2} < 0$. $\left(\frac{\tau}{\eta_g}\right)^{\frac{1}{N_e}}$ is a concave function with respect to τ. Similarly, $\left(\frac{\tau}{\eta_h}\right)^{\frac{1}{N_c}}$ is also a concave function with respect to τ. Therefore, the constraints in (45) are convex. ■

For constraints (46), we introduce two slack variables c and d to address their non-convex property, resulting in the following new constraints:

$$\ln(a)+\frac{c}{\sigma_h^2(1-\mu_h^2)}\le 0 \text{ and } \ln(b)+\frac{d}{\sigma_g^2(1-\mu_g^2)}\le 0, \tag{49}$$

$$\psi_1 \le c \text{ and } \psi_2 \le d. \tag{50}$$

Given that the constraints in (49) include logarithmic functions, we employ the SCA-based algorithm for their resolution. First, let us define

$$\varphi(a)=\ln(a), \tag{51}$$

$$\eta(b)=\ln(b), \tag{52}$$

and the first-order Taylor expansions around the points $\tilde{a}$ and $\tilde{b}$ is given as

$$\varphi(a;\tilde{a})=\varphi(\tilde{a})+\frac{a-\tilde{a}}{\tilde{a}}, \tag{53}$$

$$\eta(b;\tilde{b})=\eta(\tilde{b})+\frac{b-\tilde{b}}{\tilde{b}}, \tag{54}$$

where $\varphi(a) \le \varphi(a;\tilde{a})$ and $\eta(b) \le \eta(b;\tilde{b})$. Thus, constraints (49) can be reformulated as

$$\varphi(a;\tilde{a})+\frac{c}{\sigma_h^2(1-\mu_h^2)}\le 0, \tag{55}$$

$$\eta(b;\tilde{b})+\frac{d}{\sigma_g^2(1-\mu_g^2)}\le 0. \tag{56}$$

Furthermore, the constraints $\psi_1 \le c$ and $\psi_2 \le d$ in (50) can be rewritten as:

$$2^{\frac{R_1}{\beta}}-1\le\frac{P}{\sigma^2}\alpha c, \tag{57}$$

$$2^{\frac{R_2}{1-\beta}}-1\le\frac{P}{\sigma^2}(d-\alpha d). \tag{58}$$

For constraints (56) and (57), we have following lemma.

Lemma 4: $2^{\frac{R_1}{\beta}}$ and $2^{\frac{R_2}{1-\beta}}$ are both convex functions with respect to β.

Proof: Refer to Appendix D. ■

We also ascertain that

$$\alpha c=\frac{1}{4}(\alpha+c)^2-\frac{1}{4}(\alpha-c)^2. \tag{59}$$

Owing to the fact that $\frac{1}{4}(\alpha+c)^2$, and $\frac{1}{4}(\alpha-c)^2$ are both convex with respect to α and c. The first-order Taylor expansion of $\frac{1}{4}(\alpha+c)^2$ around the point $(\tilde{\alpha},\tilde{c})$ is computed as

$$\zeta(\alpha,c;\tilde{\alpha},\tilde{c})=\frac{1}{4}(\tilde{\alpha}+\tilde{c})^2+\frac{1}{2}(\tilde{\alpha}+\tilde{c})(\alpha-\tilde{\alpha}+c-\tilde{c}). \tag{60}$$

Thus, constraint (56) can be recast as

$$2^{\frac{R_1}{\beta}}-1\le\frac{P}{\sigma^2}\left(\zeta(\alpha,c;\tilde{\alpha},\tilde{c})-\frac{1}{4}(\alpha-c)^2\right). \tag{61}$$

Similar to (60), the first-order Taylor expansion of $\frac{1}{4}(\alpha-d)^2$ around the point $(\tilde{\alpha},\tilde{d})$ is calculated as

$$\xi(\alpha,d;\tilde{\alpha},\tilde{d})=\frac{1}{4}(\tilde{\alpha}-\tilde{d})^2+\frac{1}{2}(\tilde{\alpha}-\tilde{d})(\alpha-\tilde{\alpha}-d+\tilde{d}). \tag{62}$$

Thus, constraint (57) can be rewritten as

$$2^{\frac{R_2}{1-\beta}}-1\le\frac{P}{\sigma^2}\left(d-\frac{1}{4}(\alpha+d)^2+\xi(\alpha,d;\tilde{\alpha},\tilde{d})\right). \tag{63}$$

In the $(m+1)$-th iteration, given $\alpha^{(m)}$, $a^{(m)}$, $b^{(m)}$, $c^{(m)}$, and $d^{(m)}$ as the optimal solutions for α, a, b, c, and d from the m-th iteration, we present the following problem

$$\min_{\Xi}\ \tau \tag{64a}$$

$$\text{s.t. } \varphi(a;a^{(m)})+\frac{c}{\sigma_h^2(1-\mu_h^2)}\le 0, \tag{64b}$$

$$\eta(b;b^{(m)})+\frac{d}{\sigma_g^2(1-\mu_g^2)}\le 0, \tag{64c}$$

$$2^{\frac{R_1}{\beta}}-1\le\frac{P}{\sigma^2}\left(\zeta(\alpha,c;\alpha^{(m)},c^{(m)})-\frac{1}{4}(\alpha-c)^2\right), \tag{64d}$$

$$2^{\frac{R_2}{1-\beta}}-1\le\frac{P}{\sigma^2}\left(d-\frac{1}{4}(\alpha+d)^2+\xi(\alpha,d;\alpha^{(m)},d^{(m)})\right), \tag{64e}$$

$$(45), \tag{64f}$$

where $\Xi=\{\tau>0, 1>\alpha>0, 1>\beta>0, a>0, b>0, c>0, d>0\}$. Problem (64) is convex and can be solved using CVX.

Complexity Analysis: The complexity of updating α, β, τ, a, b, c, and d by using the interior-point method is $\mathcal{O}\left(\log\frac{1}{\delta}\right)$ [42], [43], where ϵ is the accuracy. Thus, the complexity of the SCA based algorithm is

$$\mathcal{O}\left(7L\log\frac{1}{\epsilon}\right), \tag{65}$$

where L refers to the number of iterations required for the convergence.

V. Numerical Results

In our simulation experiments, we assume $\sigma_i^2=d_i^{-\theta}$ for $i\in\{h,g\}$, where θ represents the path loss factor, and d_h and d_g denote the distances between the BS and the CU, and the distance between the BS and the EU, respectively. Specifically, we set $d_h=400$ m, $d_g=600$ m, and $\theta=3$. The power of additive Gaussian noises is denoted by $\sigma^2=-80$ dBm.

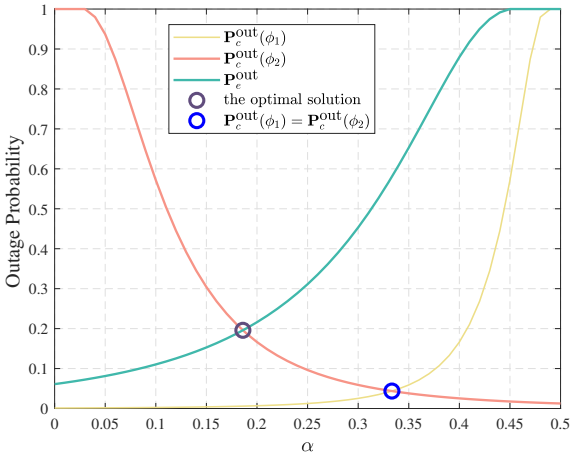

Fig. 1. Outage probability versus α for the special case in NOMA systems, where $N_c = N_e = 4$, $W_c = W_e = 5$, $R_1 = R_2 = 1$ bps/Hz, and $P = 5$ dBm.

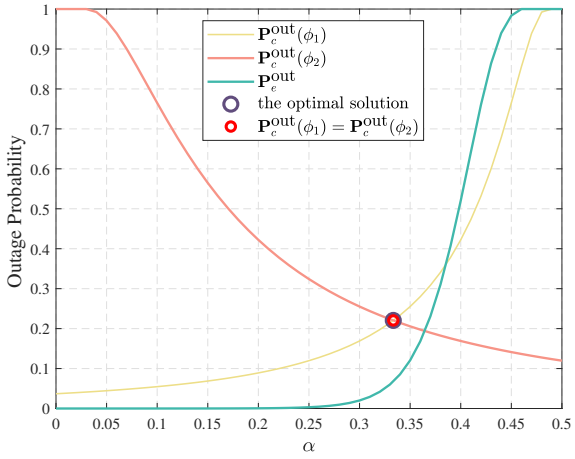

Fig. 2. Outage probability versus α for case 1 of the general case in NOMA systems, where $N_c = 2$, $N_e = 20$, $W_c = 1$, $W_e = 5$, $R_1 = R_2 = 1$ bps/Hz, and $P = 5$ dBm.

In Fig. 1, we examine the impact of the power allocation coefficient for the CU, denoted as α, on the outage probabilities of both the CU and the EU in the special case of NOMA systems, where $N_c = N_e = 4$, $W_c = W_e = 5$, $R_1 = R_2 = 1$ bps/Hz, and $P = 5$ dBm. Observations from Fig. 1 reveal that the optimal solution is $\frac{1}{1+\gamma_{th,2}+\frac{\gamma_{th,2}\sigma_h^2}{\gamma_{th,1}\sigma_g^2}} = 0.186$, and $\mathbf{P}_c^{\text{out}}(\phi_2) = \mathbf{P}_c^{\text{out}}(\phi_1)$ when $\alpha = \frac{1}{1+\gamma_{th,2}+\gamma_{th,2}/\gamma_{th,1}} = 0.3333$. These findings are in agreement with the theoretical analysis outlined in Lemma 1.

In Fig. 2 and Fig. 3, we investigate the impact of the power allocation coefficient α for the CU on the outage probabilities of the CU and the EU in NOMA systems under the general case. Analysis of Fig. 2 and Fig. 3 reveals two scenarios for optimal solutions when $N_e \neq N_c$ and $\mu_h \neq \mu_g$. Specifically, Fig. 2 illustrates the first scenario, while Fig. 3 depicts the second. In Fig. 2, the optimal solution is $\alpha = \frac{1}{1+\gamma_{th,2}+\gamma_{th,2}/\gamma_{th,1}} = 0.3333$, and in Fig. 3, a bisection search yields an optimal solution of 0.2887.

Fig. 4 illustrates the convergence behavior of our proposed SCA-based algorithm for the considered OMA systems, characterized by equal numbers of CUs and EUs *($N_c = N_e = 4$)*, bandwidths *($W_c = W_e = 5$)*, rate requirements *($R_1 = R_2 = 1$ bps/Hz)*, and transmission powers *($P = 5$ dBm, 10 dBm, and 15 dBm)*. The algorithm demonstrates rapid convergence, typically within 2 iterations, as depicted in Fig. 4.

In Fig. 5, we investigate the impact of the BS's transmit power, i.e., P, on the outage performance of OMA and NOMA systems. The parameters are set as follows: $N_c = 4$, $N_e = 6$, $W_c = 2$, $W_e = 5$ for the general case, and $N_c = N_e = 4$, $W_c = W_e = 5$ for the special case, with both R_1 and R_2 equal to 1 bps/Hz. The term "Conventional NOMA" refers to the NOMA scheme utilizing a conventional single antenna, analogous to "Conventional OMA" for the OMA scheme. The "general case" pertains to scenarios where $N_e \neq N_c$ or $\mu_h \neq \mu_g$, whereas the "special case" applies when $N_e = N_c$ and $\mu_h = \mu_g$. The notation "FAS NOMA, closed-

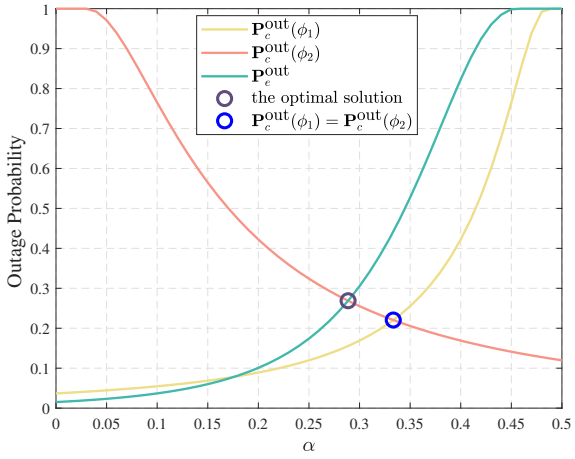

Fig. 3. Outage probability versus α for case 2 of the general case in NOMA systems, where $N_c = 2$, $N_e = 6$, $W_c = 1$, $W_e = 5$, $R_1 = R_2 = 1$ bps/Hz, and $P = 5$ dBm.

form" describes our proposed NOMA systems' closed-form solution-based scheme, employing an approximation detailed in equation (26), contrasted with "FAS NOMA" for our non-approximation-based proposals. Moreover, "FAS OMA, SCA" signifies our SCA-based algorithm for OMA systems. Observation from Fig. 5 reveals a decrease in the outage probabilities for all schemes as P escalates. Notably, the outage probabilities of FAS-based schemes are consistently lower than those of the "Conventional NOMA" scheme for $P \geq 6$ dBm, enhancing the outage probability reduction for both CU and EU, thereby improving fairness. Additionally, the performance disparity between FAS-based schemes and the "Conventional NOMA" scheme expands with increasing P. Moreover, the outage performance of "FAS NOMA, closed-form, general case" closely aligns with that of the "FAS NOMA, general case" scheme when $P \geq 20$ dBm, due to the fact that both schemes converges to the optimal solution $\frac{1}{1+\gamma_{th,2}+\gamma_{th,2}/\gamma_{th,1}}$ at $P \geq 20$ dBm.

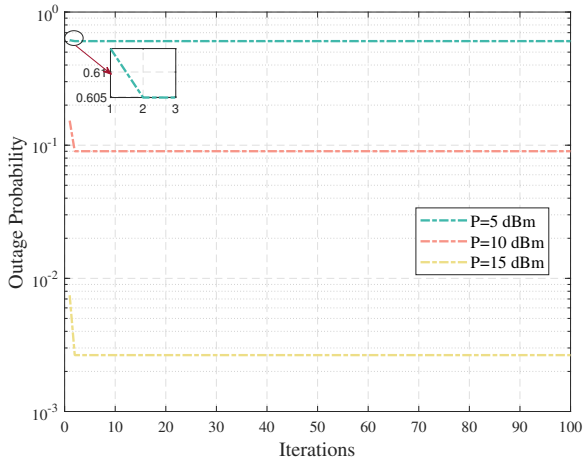

Fig. 4. Outage probability versus the number of iterations; convergence behavior of our proposed SAC based method for OMA systems, where $N_c = N_e = 4$, $W_c = W_e = 5$, $R_1 = R_2 = 1$ bps/Hz, $P = 5$ dBm, 10 dBm, and 15 dBm.

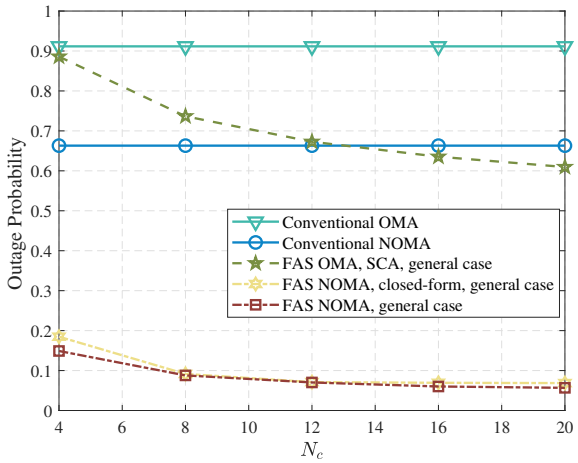

Fig. 6. Outage probability versus the number of the ports at the CU N_c for the general case in OMA and NOMA systems, where $N_e = 6$, $W_c = 5$, $W_e = 1$, $R_1 = R_2 = 1$ bps/Hz, and $P = 5$ dBm.

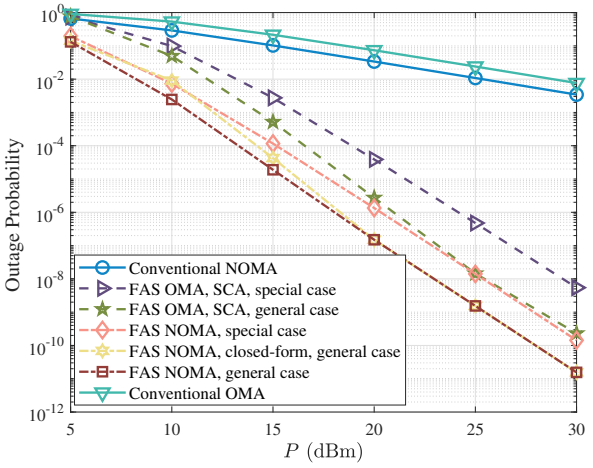

Fig. 5. Outage probability versus the transmit power of the BS P for OMA and NOMA systems, where $N_c = 4$, $N_e = 6$, $W_c = 2$, $W_e = 5$ in general case, $N_c = N_e = 4$, $W_c = W_e = 5$ in special case, and $R_1 = R_2 = 1$ bps/Hz.

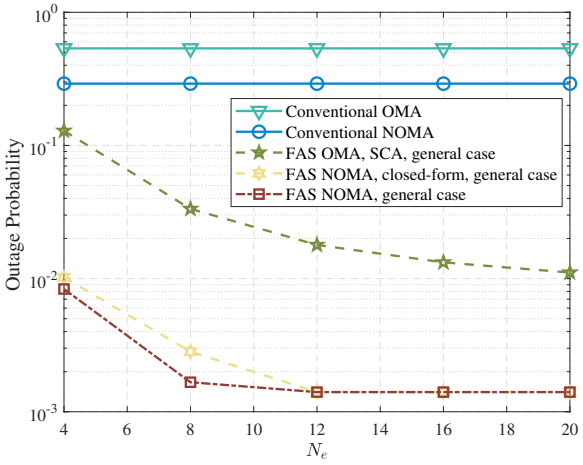

Fig. 7. Outage probability versus the number of the ports at the EU N_e for the general case in OMA and NOMA systems, where $N_c = 4$, $W_c = 1$, $W_e = 5$, $R_1 = R_2 = 1$ bps/Hz, and $P = 10$ dBm.

In Fig. 6, we present the effect of the number of the ports at the CU N_c on the outage performance of the OMA and NOMA systems, where $N_e = 6$, $W_c = 5$, $W_e = 1$, $R_1 = R_2 = 1$ bps/Hz, and $P = 5$ dBm. From Fig. 6, we can see that the outage probabilities of all schemes with FAS decreases as the N_c increases. This is because the more ports at the CU, the better the channel quality of the most favorable port. Therefore, with the increase of N_c, more power allocated to the EU to attain the better fairness between two users. However, the curve for the "Conventional NOMA" scheme remains flat since conventional NOMA cannot be able to select the ports. We can also find that the outage performance of the "FAS OMA, SCA" scheme is better than the "Conventional NOMA" scheme when $N_c \geq 13$, which indicates that the influence of the number of ports on the outage probability is significant. Besides, the outage performance of the "FAS NOMA, closed-form, general case" is close to that of the "FAS NOMA, general case" when $N_c \geq 8$.

Similar to Fig. 6, we investigate the impact of the number of the ports at the EU N_e on the outage performance of the OMA and NOMA systems in Fig. 7, where $N_c = 4$, $W_c = 1$, $W_e = 5$, $R_1 = R_2 = 1$ bps/Hz, and $P = 10$ dBm. It is found from Fig. 7 that the outage probabilities of all schemes with FAS decreases as N_e increases, since the more ports at the EU, the smaller the outage probability of the EU. The outage performance of the "FAS NOMA, closed-form, general case" scheme is the same as that of the "FAS NOMA, general case" scheme when $N_e \geq 12$. This is because the optimal solution is $\frac{1}{1+\gamma_{th,2}+\gamma_{th,2}/\gamma_{th,1}}$ for both two schemes when $N_e \geq 12$.

In Fig. 8, we investigate the effect of the target rate of the CU, denoted by R_1, on the outage performance of the OMA and NOMA systems, considering $N_c = 10$, $N_e = 4$ for the general case, and $N_c = N_e = 4$ for the special case. The settings include $W_c = W_e = 5$, $R_2 = 1$ bps/Hz,

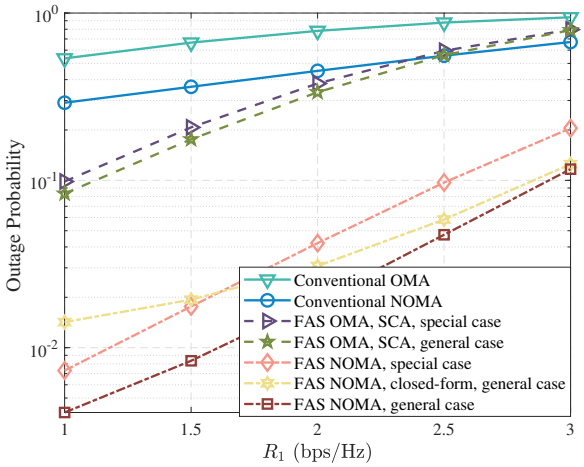

Fig. 8. Outage probability versus the target rate of the CU R_1 for OMA and NOMA systems, where $N_c = 6$, $N_e = 4$ in general case, $N_c = N_e = 4$ in special case, $W_c = W_e = 5$, $R_2 = 1$ bps/Hz, and $P = 10$ dBm.

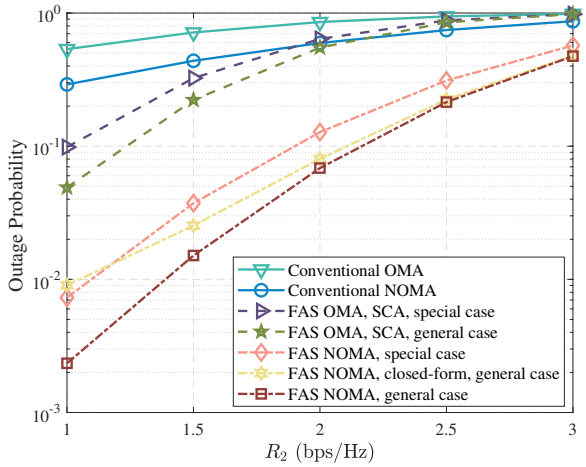

Fig. 9. Outage probability versus the target rate of the EU R_2 for OMA and NOMA systems, where $N_c = 4$, $N_e = 6$ in general case, $N_c = N_e = 4$ in special case, $W_c = W_e = 5$, $R_1 = 1$ bps/Hz, and $P = 10$ dBm.

and $P = 10$ dBm. The analysis reveals that the outage probabilities for all schemes increase with R_1. This trend is attributed to the increased power allocation to the CU. Although this reduces the outage probability for the CU, it correspondingly increases the outage probability for the EU. A comparative analysis of the "FAS NOMA, special case" scheme and "FAS NOMA, general case" scheme illustrates that an increase in N_c leads to a reduction in outage probability. The outage performance of the "FAS NOMA, closed-form, general case" scheme outperforms the "FAS NOMA, special case" scheme when $R_1 \geq 1.6$ bps/Hz. Furthermore, the performance gap between the outage performance of the "FAS NOMA, closed-form, general case" scheme and the "FAS NOMA, general case" scheme narrows as R_1 increases. This phenomenon is explained by two factors: Firstly, according to *Lemma 1*, $Q_1\left(\sqrt{\frac{2\mu_h^2}{1-\mu_h^2}}\sqrt{t}, \sqrt{\frac{2}{1-\mu_h^2}}\sqrt{\frac{\phi_2}{\sigma_h^2}}\right)$ diminishes with an increase in R_1; Secondly, a lower value of $Q_1\left(\sqrt{\frac{2\mu_h^2}{1-\mu_h^2}}\sqrt{t}, \sqrt{\frac{2}{1-\mu_h^2}}\sqrt{\frac{\phi_2}{\sigma_h^2}}\right)$ enhances the accuracy of the approximation in equation (26), making $\tilde{\mathbf{P}}_c^{\text{out}}(\phi_2)$ more precise for higher R_1 values.

In Fig. 9, we examine the influence of the EU's target rate, R_2, on the outage performance of OMA and NOMA systems, specifying $N_c = 4$, $N_e = 10$ for the general case, and $N_c = N_e = 4$ for the special case, with $W_c = W_e = 5$, $R_1 = 1$ bps/Hz, and $P = 10$ dBm. Analysis of Fig. 9 indicates that the outage probabilities for all schemes employing FAS escalate as R_2 increases. A comparative evaluation of the "FAS OMA, SCA, special case" and "FAS OMA, SCA, general case" schemes reveals that an increased N_e correlates with reduced outage probabilities. Moreover, the "FAS NOMA, closed-form, general case" scheme demonstrates superior outage performance compared to the "FAS NOMA, special case" scheme when $R_2 \geq 1.2$ bps/Hz. Additionally, the discrepancy in outage performance between the "FAS NOMA, closed-form, general case" and "FAS NOMA, general case" schemes diminishes as R_2 increases, attributed to the enhanced accuracy of $\tilde{\mathbf{P}}_e^{\text{out}}$ with higher R_2 values.

VI. Conclusion

In this paper, we considered the downlink NOMA and OMA systems, where the BS broadcasts the superposition signals to two users and both users are equipped with a single fluid antenna. We proposed the maximum outage probabilities of two user minimization problem for both NOMA and OMA systems. For the NOMA systems, we first considered the special case, i.e., $N_e = N_c$ and $\mu_h = \mu_g$, we obtained the optimal closed-form solution. Then, we obtained the optimal solution by using the bisection search for the general case, i.e., $N_e \neq N_c$ or/and $\mu_h \neq \mu_g$. For the OMA systems, we proposed the SCA based algorithm to solve the formulated problem of both the special case and the general case. Our numerical results consistently demonstrated that our proposed NOMA schemes surpass the conventional NOMA scheme. Even the performance of our proposed OMA schemes can be better than that of the conventional NOMA scheme.

Appendix A
Proof of Lemma 1

From the Leibniz integral rule

$$\frac{\partial}{\partial y}\int_{a(y)}^{b(y)} f(x,y)dx = \int_{a(y)}^{b(y)} \frac{\partial f(x,y)}{\partial y}dx + f(b(y),y)\frac{\partial b(y)}{\partial y} - f(a(y),y)\frac{\partial a(y)}{\partial y}, \tag{66}$$

we have

$$\frac{\partial \mathbf{P}_c^{\text{out}}(\phi_2)}{\partial \alpha} = \int_0^\infty e^{-t}\frac{\partial \Upsilon}{\partial \alpha}dt, \tag{67}$$

$$\frac{\partial \mathbf{P}_c^{\text{out}}(\phi_1)}{\partial \alpha} = \int_0^\infty e^{-t}\frac{\partial \Phi}{\partial \alpha}dt, \tag{68}$$

$$\frac{\partial \mathbf{P}_e^{\text{out}}}{\partial \alpha} = \int_0^\infty e^{-t}\frac{\partial \Psi}{\partial \alpha}dt, \tag{69}$$

where

$$\Upsilon = \left[1 - Q_1\left(\sqrt{\frac{2\mu^2}{1-\mu^2}}\sqrt{t}, \sqrt{\frac{2}{1-\mu^2}}\sqrt{\frac{\phi_2}{\sigma_h^2}}\right)\right]^N, \quad (70)$$

$$\Phi = \left[1 - Q_1\left(\sqrt{\frac{2\mu^2}{1-\mu^2}}\sqrt{t}, \sqrt{\frac{2}{1-\mu^2}}\sqrt{\frac{\phi_1}{\sigma_h^2}}\right)\right]^N, \quad (71)$$

$$\Psi = \left[1 - Q_1\left(\sqrt{\frac{2\mu^2}{1-\mu^2}}\sqrt{t}, \sqrt{\frac{2}{1-\mu^2}}\sqrt{\frac{\phi_1}{\sigma_g^2}}\right)\right]^N. \quad (72)$$

Taking the first-order partial derivative of Υ with respect to α, we have

$$\frac{\partial \Upsilon}{\partial \alpha} = N\left[1 - Q_1\left(\sqrt{\frac{2\mu^2}{1-\mu^2}}\sqrt{t}, \sqrt{\frac{2}{1-\mu^2}}\sqrt{\frac{\phi_2}{\sigma_h^2}}\right)\right]^{N-1} \cdot \frac{\partial\left[1 - Q_1\left(\sqrt{\frac{2\mu^2}{1-\mu^2}}\sqrt{t}, \sqrt{\frac{2}{1-\mu^2}}\sqrt{\frac{\phi_2}{\sigma_h^2}}\right)\right]}{\partial \alpha}. \quad (73)$$

Because $1-Q_1\left(\sqrt{\frac{2\mu^2}{1-\mu^2}}\sqrt{t}, \sqrt{\frac{2}{1-\mu^2}}\sqrt{\frac{\phi_2}{\sigma_h^2}}\right)$ is a monotonically increasing function with respect to $\frac{\phi_2}{\sigma_h^2}$ [44], and ϕ_2 in (16) is a monotonically decreasing function with respect to α, we have $\frac{\partial\left[1-Q_1\left(\sqrt{\frac{2\mu^2}{1-\mu^2}}\sqrt{t}, \sqrt{\frac{2}{1-\mu^2}}\sqrt{\frac{\phi_2}{\sigma_h^2}}\right)\right]}{\partial \alpha} < 0$. Therefore, we can obtain that $\frac{\partial \Upsilon}{\partial \alpha} < 0$, then $\frac{\partial \mathbf{P}_c^{\text{out}}(\phi_2)}{\partial \alpha} < 0$.

Similarly, we can find that $\frac{\partial \mathbf{P}_c^{\text{out}}(\phi_1)}{\partial \alpha} > 0$ and $\frac{\partial \mathbf{P}_e^{\text{out}}}{\partial \alpha} > 0$, since ϕ_1 is a monotonically increasing function with respect to α.

Thus, $\mathbf{P}_c^{\text{out}}(\phi_2)$ is a decreasing function with respect to α, and $\mathbf{P}_c^{\text{out}}(\phi_1)$ and $\mathbf{P}_e^{\text{out}}$ are both increasing functions with respect to α.

Appendix B
Proof of Lemma 2

Lemma 1 demonstrates that $\mathbf{P}_c^{\text{out}}(\phi_2)$ decreases with respect to α, whereas $\mathbf{P}_c^{\text{out}}(\phi_1)$ and $\mathbf{P}_e^{\text{out}}$ both increase as α increases.

Regarding Problem (21), $\mathbf{P}_c^{\text{out}}(\phi_2) = 1$ and $0 < \mathbf{P}_e^{\text{out}} < 1$ when $\alpha = 0$. Consider the inequality $\frac{\phi_1}{\sigma_h^2} < \frac{\phi_1}{\sigma_g^2}$. Given this, and noting that the function $1 - Q_1(\alpha, x)$ is monotonically increasing with respect to x, where x can represent either $\frac{\phi_1}{\sigma_h^2}$ or $\frac{\phi_1}{\sigma_g^2}$, we can deduce that $\mathbf{P}_c^{\text{out}}(\phi_2) = \mathbf{P}_c^{\text{out}}(\phi_1) < \mathbf{P}_e^{\text{out}}$ for $\alpha = \frac{1}{1+\gamma_{th,2}+\gamma_{th,2}/\gamma_{th,1}}$. Consequently, an $\hat{\alpha}$ exists such that $\mathbf{P}_c^{\text{out}}(\phi_2) = \mathbf{P}_e^{\text{out}}$ within $0 < \alpha \leq \frac{1}{1+\gamma_{th,2}+\gamma_{th,2}/\gamma_{th,1}}$. Additionally, $\max\{\mathbf{P}_c^{\text{out}}(\phi_2), \mathbf{P}_e^{\text{out}}\} = \mathbf{P}_c^{\text{out}}(\phi_2)$ for $0 < \alpha \leq \hat{\alpha}$, and $\max\{\mathbf{P}_c^{\text{out}}(\phi_2), \mathbf{P}_e^{\text{out}}\} = \mathbf{P}_e^{\text{out}}$ for $\hat{\alpha} < \alpha \leq \frac{1}{1+\gamma_{th,2}+\gamma_{th,2}/\gamma_{th,1}}$. Therefore, $\max\{\mathbf{P}_c^{\text{out}}(\phi_2), \mathbf{P}_e^{\text{out}}\}$ initially decreases, then increases with α, making $\hat{\alpha}$ the optimal solution for Problem (21). Given $\frac{\phi_2}{\sigma_h^2} = \frac{\phi_1}{\sigma_g^2}$, $\hat{\alpha}$ is expressed as

$$\hat{\alpha} = \frac{1}{1 + \gamma_{th,2} + \frac{\gamma_{th,2}\sigma_h^2}{\gamma_{th,1}\sigma_g^2}}. \quad (74)$$

For Problem (22), noting that $\frac{\phi_1}{\sigma_h^2} < \frac{\phi_1}{\sigma_g^2}$ and $1 - Q_1(\alpha, x)$ increases with x, $\mathbf{P}_c^{\text{out}}(\phi_1) < \mathbf{P}_e^{\text{out}}$ when α lies between $\frac{1}{1+\gamma_{th,2}+\gamma_{th,2}/\gamma_{th,1}}$ and $\frac{1}{1+\gamma_{th,2}}$. Thus, $\max \mathbf{P}_c^{\text{out}}(\phi_1), \mathbf{P}_e^{\text{out}} = \mathbf{P}_e^{\text{out}}$ within this range. The optimum value for Problem (22) exceeds $\mathbf{P}_e^{\text{out}}$ when $\alpha = \frac{1}{1+\gamma_{th,2}+\gamma_{th,2}/\gamma_{th,1}}$.

In conclusion, the optimal solution for Problem (20) is determined to be $\hat{\alpha}$.

Appendix C
Proof of Theorem 1

After some mathematical manipulation, $\tilde{\mathbf{P}}_c^{\text{out}}(\phi_2) = \tilde{\mathbf{P}}_e^{\text{out}}$ can be rewritten as

$$a_1 d_1 \alpha^2 + (b_1 d_1 + c_1 - a_1)\alpha - b_1 = 0, \quad (75)$$

where

$$a_1 = \ln(N_e/N_c), \quad (76)$$

$$b_1 = \frac{\gamma_{th,1}\sigma^2}{P\sigma_h^2}, \quad (77)$$

$$c_1 = \frac{\gamma_{th,2}\sigma^2}{P\sigma_g^2}, \quad (78)$$

$$d_1 = 1 + \gamma_{th,2}. \quad (79)$$

When $N_c = N_e$, i.e., $a_1 = 0$, according to (75), we can obtain that

$$\alpha = \frac{1}{1 + \gamma_{th,2} + \frac{\gamma_{th,2}\sigma_h^2}{\gamma_{th,1}\sigma_g^2}}, \quad (80)$$

When $N_c \neq N_e$, we know two possible solutions to equation (75) are given by

$$\alpha_1 = \frac{-(b_1 d_1 + c_1 - a_1) + \sqrt{(b_1 d_1 + c_1 - a_1)^2 + 4 b_1 a_1 d_1}}{2 a_1 d_1}, \quad (81)$$

$$\alpha_2 = \frac{-(b_1 d_1 + c_1 - a_1) - \sqrt{(b_1 d_1 + c_1 - a_1)^2 + 4 b_1 a_1 d_1}}{2 a_1 d_1}. \quad (82)$$

Appendix D
Proof of Lemma 3

Taking the first-order partial derivative and the second-order partial derivative of $2^{\frac{R_1}{\beta}}$ with respect to β, we have

$$\frac{\partial 2^{\frac{R_1}{\beta}}}{\partial \beta} = -2^{\frac{R_1}{\beta}} \frac{R_1 \ln 2}{\beta^2}, \quad (83)$$

$$\frac{\partial^2 2^{\frac{R_1}{\beta}}}{\partial \beta^2} = 2^{\frac{R_1}{\beta}} \frac{R_1^2 (\ln 2)^2}{\beta^4} + 2^{\frac{R_1}{\beta}} \frac{2 R_1 \ln 2}{\beta^3}. \quad (84)$$

Taking the first-order partial derivative and the second-order partial derivative of $2^{\frac{R_2}{1-\beta}}$ with respect to β, we have

$$\frac{\partial 2^{\frac{R_2}{1-\beta}}}{\partial \beta} = 2^{\frac{R_2}{(1-\beta)}} \frac{R_2 \ln 2}{(1-\beta)^2}, \quad (85)$$

$$\frac{\partial^2 2^{\frac{R_2}{1-\beta}}}{\partial \beta^2} = 2^{\frac{R_2}{(1-\beta)}} \frac{R_2^2 (\ln 2)^2}{(1-\beta)^4} + 2^{\frac{R_2}{(1-\beta)}} \frac{2 R_2 \ln 2}{(1-\beta)^3}. \quad (86)$$

Because $\frac{\partial^2 2^{\frac{R_1}{\beta}}}{\partial \beta^2} > 0$ and $\frac{\partial^2 2^{\frac{R_2}{1-\beta}}}{\partial \beta^2} > 0$, $2^{\frac{R_1}{\beta}}$ and $2^{\frac{R_2}{1-\beta}}$ are both convex functions with respect to β.

REFERENCES

[1] A. Giridhar and P. R. Kumar, "Toward a theory of in-network computation in wireless sensor networks," *IEEE Commun. Mag.*, vol. 44, no. 4, pp. 98-107, Apr. 2006.

[2] K. W. Choi, A. A. Aziz, D. Setiawan, N. M. Tran, L. Ginting, and D. I. Kim, "Distributed wireless power transfer system for Internet of Things devices," *IEEE Internet Things J.*, vol. 5, no. 4, pp. 2657-2671, Aug. 2018.

[3] G. J. Foschini and M. J. Gans, "On limits of wireless communications in a fading environment when using multiple antennas," *Wireless Pers. Commun.*, vol. 6, no. 3, pp. 311-335, Mar. 1998.

[4] L. Zheng and D. N. C. Tse, "Diversity and multiplexing: A fundamental tradeoff in multiple-antenna channels," *IEEE Trans. Inf. Theory*, vol. 49, no. 5, pp. 1073-1096, May 2003.

[5] J. Zheng, Q. Zhang, and J. Qin, "Average achievable rate and average BLER analyses for MIMO short-packet communication systems," *IEEE Trans. Veh. Technol.*, vol. 70, no. 11, pp. 12238-12242, Nov. 2021.

[6] K.-K. Wong, A. Shojaeifard, K.-F. Tong, and Y. Zhang, "Fluid antenna system," *IEEE Trans. Wireless Commun.*, vol. 20, no. 3, pp. 1950-1962, Mar 2021.

[7] M. Khammassi, A. Kammoun and M. -S. Alouini, "A new analytical approximation of the fluid antenna system channel," *IEEE Trans. Wireless Commun.*, vol. 22, no. 12, pp. 8843-8858, Dec. 2023.

[8] K.-K. Wong, K.-F. Tong, Y. Shen, Y. Chen, and Y. Zhang, "Bruce Lee inspired fluid antenna system: Six research topics and the potentials for 6G," *Frontiers Commun. Netw.*, vol. 3, no. 853416, pp. 1-31, Mar. 2022.

[9] Y. Huang, L. Xing, C. Song, S. Wang, and F. Elhouni, "Liquid antennas: Past, present and future," *IEEE Open J. Antennas Propag.*, vol. 2, pp. 473487, Mar. 2021.

[10] K.-K. Wong, A. Shojaeifard, K.-F. Tong and Y. Zhang, "Performance limits of fluid antenna systems," *IEEE Commun. Letters*, vol. 24, no. 11, pp. 2469-2472, Nov. 2020.

[11] X. Lai, T. Wu, J. Yao, C. Pan, M. Elkashlan, and K.-K. Wong, "On performance of fluid antenna system using maximum ratio combining," *IEEE Commun. Lett.*, early access, 2023, doi: 10.1109/LCOMM.2023.3348028.

[12] H. Xu, G. Zhou, K.-K. Wong, W. New, C. Wang, C.-B. Chae, R. Murch, S. Jin, and Y. Zhang, "Channel estimation for FAS-assisted multiuser mmWave systems," *IEEE Commun. Lett.*, early access, 2023, doi: 10.1109/LCOMM.2023.3347951.

[13] Z. Chai, K.-K. Wong, K.-F. Tong, Y. Chen, and Y. Zhang, "Port selection for fluid antenna systems," *IEEE Commun. Lett.*, vol. 26, no. 5, pp. 1180-1184, May 2022.

[14] Y. Ye, L. You, J. Wang, H. Xu, K.-K. Wong, and X. Gao, "Fluid antenna-assisted MIMO transmission exploiting statistical CSI," *IEEE Commun. Lett.*, early access, 2023, doi: 10.1109/LCOMM.2023.3336805.

[15] B. Tang, H. Xu, K.-K. Wong, K.-F. Tong, Y. Zhang, and C.-B. Chae, "Fluid antenna enabling secret communications," *IEEE Commun. Lett.*, vol. 27, no. 6, pp. 1491-1495, Jun. 2023.

[16] K.-K. Wong and K.-F. Tong, "Fluid antenna multiple access," *IEEE Trans. Wireless Commun.*, vol. 21, no. 7, pp. 4801-4815, Jul. 2022.

[17] K.-K. Wong, D. Morales-Jimenez, K.-F. Tong, and C.-B. Chae, "Slow fluid antenna multiple access," *IEEE Trans. Commun.*, vol. 71, no. 5, pp. 2831-2846, May 2023.

[18] N. Waqar, K.-K. Wong, K.-F. Tong, A. Sharples, and Y. Zhang, "Deep learning enabled slow fluid antenna multiple access," *IEEE Commun. Lett.*, vol. 27, no. 3, pp. 861-865, Mar. 2023.

[19] K.-K. Wong, K.-F. Tong, Y. Chen, Y. Zhang, and C.-B. Chae, "Opportunistic fluid antenna multiple access," *IEEE Trans. Wireless Commun.*, vol. 22, no. 11, pp. 7819-7833, Nov. 2023.

[20] L. Dai, B. Wang, Y. Yuan, S. Han, I. Chih-lin, and Z. Wang, "Non-orthogonal multiple access for 5G: solutions, challenges, opportunities, and future research trends," *IEEE Commun. Mag.*, vol. 53, no. 9, pp. 74–81, Sep. 2015.

[21] Z. Ding, X. Lei, G. K. Karagiannidis, R. Schober, J. Yuan, and V. K. Bhargava, "A survey on non-orthogonal multiple access for 5G networks: Research challenges and future trends," *IEEE J. Sel. Areas Commun.*, vol. 35, no. 10, pp. 2181–2195, Oct. 2017.

[22] J. Yao, Q. Zhang, and J. Qin, "Joint decoding in downlink NOMA systems with finite blocklength transmissions for ultrareliable low-latency tasks," *IEEE Internet Things J.*, vol. 9, no. 18, pp. 1770517713, Sep. 2022.

[23] Y. Liu, S. Zhang, X. Mu, Z. Ding, R. Schober, N. AlDhahir, E. Hossain, and X. Shen, "Evolution of NOMA toward next generation multiple access (NGMA) for 6G," *IEEE J. Sel. Areas Commun.*, vol. 40, no. 4, pp. 1037–1071, Apr. 2022.

[24] J. Zuo, Y. Liu, Z. Qin, and N. Al-Dhahir, "Resource allocation in intelligent reflecting surface assisted NOMA systems," *IEEE Trans. Commun.*, vol. 68, no. 11, pp. 7170–7183, Nov. 2020.

[25] Y. Li, M. Jiang, Q. Zhang, Q. Li, and J. Qin, "Cooperative non-orthogonal multiple access in multiple-input-multiple-output channels," *IEEE Trans. Wireless Commun.*, vol. 17, no. 3, pp. 2068-2079, Mar. 2018.

[26] Y. Sun, D. W. K. Ng, Z. Ding, and R. Schober, "Optimal joint power and subcarrier allocation for full-duplex multicarrier non-orthogonal multiple access systems," *IEEE Trans. Commun.*, vol. 65, no. 3, pp. 1077-1091, 2017.

[27] T. Hou, Y. Liu, Z. Song, X. Sun, Y. Chen, and L. Hanzo, "Reconfigurable intelligent surface aided NOMA networks," *IEEE J. Sel. Areas Commun.*, vol. 38, no. 11, pp. 2575-2588, Nov. 2020.

[28] T. Hou, Y. Liu, Z. Song, X. Sun, and Y. Chen, "NOMA-enhanced terrestrial and aerial IoT networks with partial CSI," *IEEE Internet Things J.*, vol. 7, no. 4, pp. 3254-3266, Apr. 2020.

[29] P. Swami, M. K. Mishra, V. Bhatia, and T. Ratnarajah, "Performance analysis of NOMA enabled hybrid network with limited feedback," *IEEE Trans. Veh. Technol.*, vol. 69, no. 4, pp. 4516-4521, Apr. 2020.

[30] Y. Yapici, I. Guvenc, and H. Dai, "Low-resolution limited-feedback NOMA for mmWave communications," *IEEE Trans. Wireless Commun.*, vol. 19, no. 8, pp. 5433-5446, Aug. 2020.

[31] Z. Ding, Z. Yang, P. Fan, and H. V. Poor, "On the performance of non-orthogonal multiple access in 5G systems with randomly deployed users," *IEEE Signal Process. Lett.*, vol. 21, no. 12, pp. 1501-1505, Dec. 2014.

[32] X. Wang, J. Wang, L. He, and J. Song, "Outage analysis for downlink NOMA with statistical channel state information," *IEEE Wireless Commun. Lett.*, vol. 7, no. 2, pp. 142-145, Apr. 2018.

[33] S. Li, M. Derakhshani, S. Lambotharan, and L. Hanzo, "Outage probability analysis for the multi-carrier NOMA downlink relying on statistical CSI," *IEEE Trans. Commun.*, vol. 68, no. 6, pp. 3572-3587, Jun. 2020.

[34] C. Skouroumounis and I. Krikidis, "Fluid antenna with linear MMSE channel estimation for large-scale cellular networks," *IEEE Trans. Commun.*, vol. 71, no. 2, pp. 11121125, Feb. 2023.

[35] L. Tlebaldiyeva, S. Arzykulov, T. A. Tsiftsis, and G. Nauryzbayev, "Full-duplex cooperative NOMA-based mmWave networks with fluid antenna system (FAS) receivers," in *Proc. Int. Balkan Conf. Commun. Netw. (BalkanCom)*, pp. 16, 5-8 Jun. 2023, Istanbul, Turkey.

[36] J. Zheng, T. Wu, X. Lai, C. Pan, M. Elkashlan, K.-K. Wong, "FAS-assisted NOMA short-packet communication systems," [Online] arXiv preprint arXiv:2310.14251, 2023

[37] W. New, K.-K. Wong, H. Xu, K.-F. Tong, C.-B. Chae, and Y. Zhang, "Fluid antenna system enhancing orthogonal and non-orthogonal multiple access," *IEEE Commun. Lett.*, early access, 2023, doi: 10.1109/LCOMM.2023.3333313.

[38] R. Jiao and L. Dai, "On the max-min fairness of beamspace MIMO-NOMA," *IEEE Trans. Signal Process.*, vol. 68, pp. 49194932, 2020.

[39] S. Shi, L. Yang, and H. Zhu, "Outage balancing in downlink nonorthogonal multiple access with statistical channel state information," *IEEE Trans. Wireless Commun.*, vol. 15, no. 7, pp. 4718-4731, 2016.

[40] X. Zhang, T. Chang, Y. Liu, C. Shen, and G. Zhu, "Max-min fairness user scheduling and power allocation in full-duplex OFDMA systems," *IEEE Trans. Wireless Commun.*, vol. 18, no. 6, pp. 3078-3092, Jun. 2019.

[41] I. S. Gradshteyn and I. M. Ryzhik, *Table of Integrals, Series, and Products, 7th ed.* San Diego, CA: Academic, 2007

[42] S. Boyd and L. Vandenberghe, *Convex Optimization*. Cambridge, U.K.: Cambridge Univ. Press, 2004.

[43] I. Polik and T. Terlaky, "Interior point methods for nonlinear optimization," in *Nonlinear Optimization*, G. Di Pillo and F. Schoen, Eds., 1st ed. New York, NY, USA: Springer, 2010, ch. 4.

[44] M. K. Simon and M.-S. Alouini, "Exponential-type bounds on the generalized Marcum Q-function with application to error probability analysis over fading channels" *IIEEE Trans. on Commun.*, vol. 48, pp. 359-366, Mar. 2000.